

RESEARCH PAPER

Enhanced cytotoxicity of auraptene to prostate cancer cells by dextran-coated Fe₃O₄ nanoparticles

Narges Naseri¹, Mehrdad Iranshahi², Zahra Tayarani-Najaran³, Saleh Rakhshani⁴, Leila Mohtashami^{1*}

¹Department of Pharmacognosy, School of Pharmacy, Mashhad University of Medical Sciences, Mashhad, Iran

²Biotechnology Research Center, Pharmaceutical Technology Institute, Mashhad University of Medical Sciences, Mashhad, Iran

³Targeted Drug Delivery Research Center, Pharmaceutical Technology Institute, Mashhad University of Medical Sciences, Mashhad, Iran

⁴Department of Pharmaceutics, School of Pharmacy, Mashhad University of Medical Sciences, Mashhad, Iran

ABSTRACT

Objective(s): Auraptene (AUR) is a monoterpene coumarin compound with several biological activities specifically anti-cancer. The bioavailability of AUR in biological fluids is negligible, thus, the cytotoxicity of this compound for the target cells is low. Herein, the synthesis of AUR-coated Fe₃O₄ nanoparticles is presented as a strategy to increase the cytotoxicity of AUR on PC3, DU145, and LNCaP prostate cancer cells.

Materials and Methods: Fe₃O₄ nanoparticles were synthesized via co-precipitation method, coated with AUR and stabilized by dextran. They were characterized by X-ray diffraction spectroscopy (XRD), Fourier-transform infrared spectroscopy (FTIR), scanning electron microscopy (SEM), dynamic light scattering (DLS) analysis, and vibrating sample magnetometry (VSM). In vitro release test for coated nanoparticles was performed in both physiologic (pH= 7.4) and acidic (pH= 5.5) environments. Cytotoxicity for prostate cancer cells was evaluated by AlamarBlue assay and the results were analyzed by one-way and two-way ANOVA tests.

Results: Characterization outcomes represented the formation of magnetic nanoparticles with good crystalline structure, relatively spherical shape and superparamagnetic properties. AUR release profile from nanoparticles demonstrated that coated nanoparticles are able to inhibit burst release of this compound. AUR release was remarkably higher in acidic medium that can be advantageous for treating tumor regions. Cytotoxicity results indicated that AUR had a very low toxicity against prostate cancer cells at the tested concentrations. In contrast, AUR-coated Fe₃O₄ nanoparticles were significantly cytotoxic on all the cell lines.

Conclusion: The coating of AUR on the surface of Fe₃O₄ nanoparticles was a successful approach to enhance the efficacy and cytotoxicity of this compound.

Keywords: Auraptene; Coumarin; Cytotoxicity; Fe₃O₄ nanoparticles; Prostate cancer

How to cite this article

Naseri N, Iranshahi M, Tayarani-Najaran Z, Rakhshani S, Mohtashami L. Enhanced cytotoxicity of auraptene to prostate cancer cells by dextran-coated Fe₃O₄ nanoparticles. *Nanomed J.* 2022; 8(1): 77-86. DOI: [10.22038/NMJ.2022.61479.1633](https://doi.org/10.22038/NMJ.2022.61479.1633)

INTRODUCTION

Prostate cancer is the third deadliest cancer in men [1]. Genetics [2], prostatitis and environmental risk factors have a key role in the prevalence of this disease [3]. Several treatment modalities such as radiotherapy, chemotherapy, surgery and hormonal therapy have been used

to manage prostate cancer, however, the effect of these treatments is still limited and the toxicity of anti-cancer agents is high [4]. Auraptene (AUR) is a monoterpene coumarin compound that is mostly isolated from *Citrus* and *Ferula* species [5]. This compound exerts various pharmacological activities including anti-diabetic [6, 7], immunomodulatory [8, 9], pigmentation-modulatory [10], anti-inflammatory [11], neuroprotective [12-14], and anti-cancer [15-17]. While the cytotoxicity of AUR to PC3, DU145 and LNCaP prostate cancer cells

* Corresponding Author Email: mohtashamil941@mums.ac.ir; leila.mohtashami90@gmail.com

Note. This manuscript was submitted on October 5, 2021; approved on December 8, 2021

has been significant to a certain degree [4, 18], the poor solubility of this compound restricts its further clinical applicability. Therefore, it is essential to design delivery systems that can improve AUR uptake and efficacy.

Nanotechnology has a great potential in developing nanomaterials for medicinal, physical, and chemical applications. Recent nanotechnology developments in pharmaceutical and biomedical fields have led to a revolution in drug delivery systems [19, 20]. A nanomaterial is considered a manufactured, natural or incidental product containing particles where 50% or more of the particles are between 1 to 100 nm [21]. Nanoparticles (NPs) can be classified into four groups: carbon-based, inorganic-based, organic-based, and composite-based [22]. Metal and metal oxide NPs are inorganic-based NPs that are synthesized from several metals including silver, iron, titanium, calcium, and magnesium [23]. Among these metal oxide NPs, iron oxide magnetic nanoparticles (MNPs) have gained special attention due to their simple and low cost production, good compatibility, eco-friendliness and magnetic properties [24]. Therefore, they are considered as an ideal nanosystem for biomedical applications [25] like MRI [26], hyperthermia [27], tissue repair, cell labeling and magnetofection [28]. Beyond these applications, drug delivery using iron oxide MNPs as carriers has been of great interest in recent years. Conjugating natural products on their surface enhances the therapeutic effects of these potential drugs [29] since poor uptake and nonspecific delivery of natural compounds are overcome [30]. The most commonly used MNPs for medical applications are Fe_3O_4 and $\gamma\text{-Fe}_2\text{O}_3$ NPs [31]. To synthesize these NPs, different methods have been used among which co-precipitation is one of the most efficient and simple ways [32].

Iron oxide NPs are extremely prone to subsequent aggregation and instability after synthesis leading to their elimination by endoplasmic reticulum [24]. As a result, the surface of MNPs should be coated by biofunctional coatings to protect against their degradation and improve water dispersibility, biodistribution and pharmacokinetic properties of these nanoparticles [33]. Among various organic and inorganic coatings, special attention is being paid to natural surfactants such as Gum Arabic [34] or biocompatible polymers like starch [35], polyvinyl alcohol (PVA) [36], polyethylene glycol

(PEG) [37, 38], chitosan [39-41], and dextran [42, 43]. Dextran is biocompatible and biodegradable and can enhance stability leading to a longer blood circulation time [44]. Dextran appears to possess a favorable chain size, enabling it to have optimum polar interactions (hydrogen bonding and chelation) with the surface of MNPs. Single hydrogen bonds are weak, but numerous hydroxyl groups per dextran molecule can result in a high total bonding energy of hydrogen bonds [45]. Therefore, dextran can be considered as an eligible polymer for stabilizing Fe_3O_4 MNPs.

In this study, Fe_3O_4 nanoparticles were synthesized by co-precipitation method and coated with AUR and dextran. Then, the anti-proliferative effect of the coated nanoparticles was evaluated and compared with AUR on three prostate cancer cell lines including PC3, DU145 and LNCaP. We assume that Fe_3O_4 MNPs may ameliorate the penetration of AUR into the cancer cells, thus, increasing its cytotoxicity.

MATERIALS AND METHODS

Materials

$\text{FeCl}_2 \cdot 4\text{H}_2\text{O}$, $\text{FeCl}_3 \cdot 6\text{H}_2\text{O}$, HCl 37%, NH_3 25%, and dimethyl sulfoxide (DMSO) were purchased from Merck (Germany), dextran (MW: 15000-25000), AlamarBlue and RPMI-1640 medium from Sigma-Aldrich (USA), penicillin-streptomycin (Pen-Strep) and fetal bovine serum (FBS) from Gibco (USA), doxorubicin (DOX) from EbewePharma (Austria), AUR from Golexir Pars (Iran) and prostate cancer cell lines (PC3, DU145, and LNCaP) from Pasteur Institute (Iran).

Synthesis of AUR-coated magnetic nanoparticles and their stabilization

To synthesize Fe_3O_4 MNPs, $\text{FeCl}_3 \cdot 6\text{H}_2\text{O}$ and $\text{FeCl}_2 \cdot 4\text{H}_2\text{O}$ were dissolved in deionized (DI) water at a molar ratio of 2:1 under a temperature of 70°C while the argon gas was bubbling. Then a basic solution of NH_3 in DI water was added, drop by drop, to the mixture at 265 rpm. The color change of the dispersion from dark brown to black is the sign of Fe_3O_4 nanoparticles formation. The nanoparticles were separated by a strong magnet and washed several times with DI water.

To load AUR on the surface of MNPs, we dispersed 100 mg of Fe_3O_4 MNPs in 100 mL of DI water and sonicated the whole solution for 10 min. A 60 mg/2 mL DMSO solution of AUR was added drop by drop to the dispersion at 300 rpm

and 45°C for 15 min. Coated MNPs were separated by a strong magnet and washed with DI water to eliminate uncoated AUR. 150 mg of dextran was dissolved in 100 mL of DI water and added to AUR-coated MNPs and the solution was sonicated for 2 min. The dispersion was stirred at a temperature of 80-90°C and a speed of 256 rpm for 4 hr. This was followed by another stirring process at 400 rpm for 24 hr. The resulting dispersion (dextran@AUR-coated MNPs) was freeze-dried and used for characterization tests, release test and cytotoxicity evaluation on PC3, DU145 and LNCaP cell lines. Dextran@Fe₃O₄ MNPs (drug-free nanoparticles) were synthesized by the same method except that the AUR coating step was not performed.

Characterization tests

The crystalline structure of different samples was studied by X-ray diffraction (XRD) measurements (Bruker, D8). Surface chemistry was studied by Fourier-transform infrared (FTIR) spectroscopy (Perkin-Elmer, Paragon 1000). Morphology was investigated by scanning electron microscopy (SEM) (Hitachi, S-4160) and transmission electron microscopy (TEM) (Philips, CM 30). Hydrodynamic diameter, polydispersity index, zeta potential and colloidal stability of dextran@AUR-coated MNPs dispersion were analyzed by particle size analyzer (Malvern, Zeta sizer-nano ZS). Magnetic properties were determined by vibrating-sample magnetometry (VSM) (MDK). All the experiments were performed at 25°C.

Determination of encapsulation efficiency and AUR loading

1 mg of dextran@AUR-coated MNPs was dispersed in 1 mL of DMSO, sonicated for 5 min and centrifuged at 10000 rpm for 20 min. The drug concentration in the supernatant was evaluated according to the specific ultraviolet (UV) absorbance of AUR at 322.7 nm in a UV-Vis spectrometer. The encapsulation efficiency was calculated using:

$$\text{Encapsulation efficiency}\% = \frac{w_s}{w} \times 100$$

where, “w_s” and “w” are the weights of the coated AUR and the total added AUR to the dispersion, respectively. AUR loading was calculated using:

$$\text{AUR loading}\% = \frac{w_s}{w} \times 100$$

where, “w_s” and “w” are the weights of the

coated AUR and coated nanoparticles, respectively.

In vitro release studies

To study AUR release, we suspended 1 mg of dextran@AUR-coated MNPs (containing 63.36 µg of AUR) in 564 mL of phosphate-buffered saline (PBS, pH= 7.4) and citrate buffer (pH= 5.5) both containing 0.1% w/w Tween-80. Also, 63.36 µg of AUR was suspended in the same amount of Tween-containing PBS for investigating the dissolution profile of free drug. The samples were placed in a shaker-incubator at a temperature of 37°C and a speed of 100 rpm. 300 µL of PBS and citrate buffer media were withdrawn after 0, 0.5, 1, 3, 6, 9, 12, 24, 48, 72, 96 and 120 hr for evaluating AUR release from coated nanoparticles and 300 µL of PBS medium was withdrawn after 0, 0.5, 1 and 3 hours for evaluating the dissolution profile of AUR. Both physiologic and acidic environments were replenished with 300 µL of fresh medium after each sampling. The quantity of released AUR at different times was measured by spectrofluorometry at 329 nm as excitation wavelength and 390 nm as emission wavelength. Each test was repeated three times. To compare the differences in the release profile of AUR in physiologic and acidic pH, the results of drug release versus time were fit to kinetic models using the KineticDS software. Besides, mean dissolution time (MDT) parameter was used for comparing the dissolution rate of our extended-release dosage form in both media. MDT was calculated using [46]:

$$\text{MDT} = \frac{\int_0^{\infty} (M_{\infty} - M(t)) dt}{M_{\infty}}$$

Where M indicates the mass of drug release in the time of t.

In vitro cytotoxicity test

Human prostate cancer cell lines (PC3, DU145 and LNCaP) were seeded in 96-well plates (RPMI-1640 medium containing 10% FBS and 1% Pen-Strep) with a density of 1×10⁴ cells/well and incubated at 5% CO₂ and a temperature of 37°C for 24 hr. A stock solution (60 mg/mL) of AUR was prepared in DMSO and diluted with the culture medium to ensure that the concentration of DMSO in different AUR concentrations is less than 0.1%. The cells were treated by DOX at (0.1 µg/mL), AUR at (0.1-10 µg/mL), dextran@AUR-coated MNPs (with a series of 0.1-10 µg/mL of final AUR

concentration) and dextran@Fe₃O₄ MNPs (with the same amount as dextran@AUR-coated MNPs). The untreated cells served as negative control whereas DOX-treated cells served as positive control. After 72 hr, AlamarBlue was added to each well and the plates were incubated until the reduction reaction was terminated. The absorbance was measured at 600 nm with microplate reader (Biotek, Epoch) and the viability percentage was calculated. This experiment was repeated three times each in triplicate for the tested cell lines.

RESULTS AND DISCUSSION

Characterization tests

XRD patterns for Fe₃O₄ MNPs and dextran@AUR-coated MNPs are shown in Fig 1. Both

patterns have similar peaks to those of the “The Joint Committee on Powder Diffraction Standards (JCPDS)” reference pattern of Fe₃O₄ nanoparticles (No. 85-1436). Fe₃O₄ nanoparticles (Fig 1a) have sharp (311) and (440) peaks as a result of their high crystalline structure [47]. The same pattern with peaks of lower intensities can be seen for dextran@AUR-coated MNPs (Fig 1b), demonstrating an efficient coating with no changes in their crystalline structure. The size of the coated and uncoated nanoparticles was calculated according to the Scherrer equation and determined to be 13.498 nm for Fe₃O₄ MNPs and 16.339 nm for dextran@AUR-coated MNPs. The FTIR spectrum of Fe₃O₄ MNPs (Fig. 2) indicated Fe-O vibration bands at 573 cm⁻¹. The bending vibrations at 1653 cm⁻¹ and

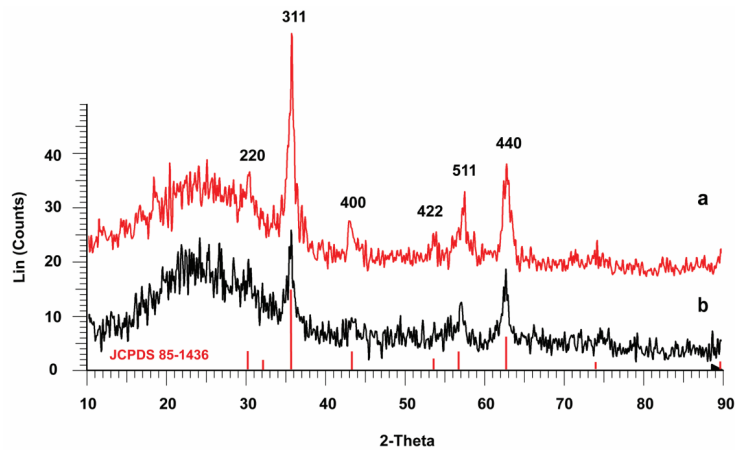


Fig 1. XRD patterns for Fe₃O₄ MNPs (a) and dextran@AUR-coated MNPs (b)

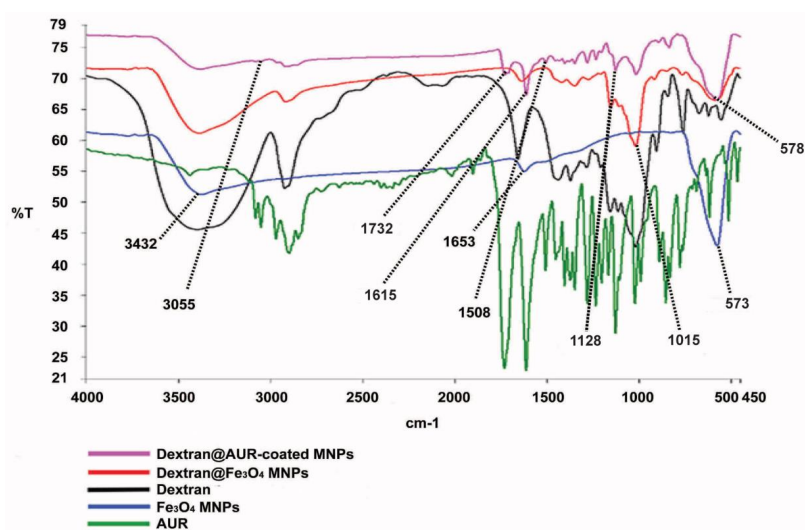


Fig 2. FTIR spectra for samples AUR, Fe₃O₄ MNPs, dextran, dextran@Fe₃O₄ MNPs and dextran@AUR-coated MNPs

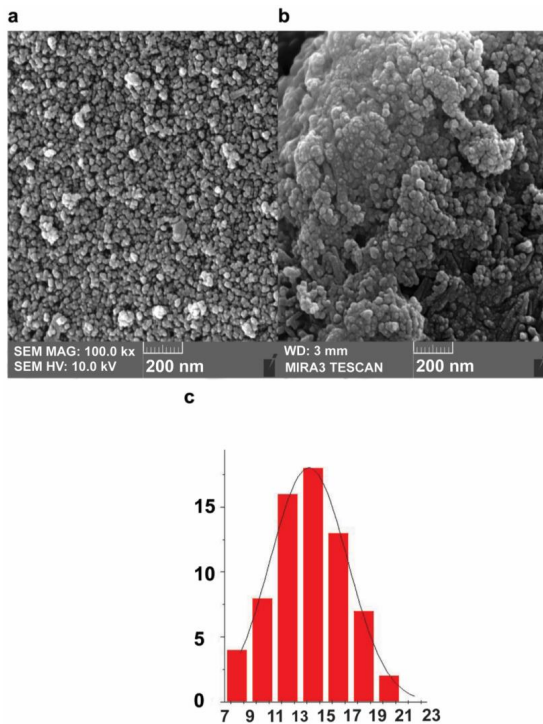


Fig 3. SEM image of Fe₃O₄ MNPs (a) and dextran@AUR-coated MNPs (b) and the relative size distribution graph of coated MNPs (c)

stretching vibrations at 3432 cm⁻¹ are due to the water molecules adsorbed on the surface of MNPs [48]. In the spectrum of dextran@Fe₃O₄ MNPs and dextran@AUR-coated MNPs, the wavelength of Fe-O band was shifted from 573 cm⁻¹ to 578 cm⁻¹, possibly due to the surface interactions between dextran and magnetic nanoparticles. Also, the peaks at 1015 cm⁻¹ and 1128 cm⁻¹ are due to C^{OH} stretching vibrations and C-H bending vibrations, respectively, indicating that dextran was well placed on the surface of nanoparticles [49]. The probable mechanism of dextran adsorption may be the hydrogen bonds between the hydroxyl moiety present in dextran and on the surface of nanoparticles. In the spectrum of dextran@AUR-coated MNPs, the stretching vibrations of phenyl protons in the coumarin ring at 3055 cm⁻¹ [50], carbonyl group at 1732 cm⁻¹ and double bonds at 1508 and 1615 cm⁻¹ [51] of AUR are present. This shows the successful coating of AUR on the surface of dextran@AUR-coated MNPs. Investigating the morphology of Fe₃O₄ MNPs (Fig. 3a) and dextran@AUR-coated MNPs (Fig 3b) by SEM showed that both particles were almost spherical with high agglomeration tendency as a result of the small

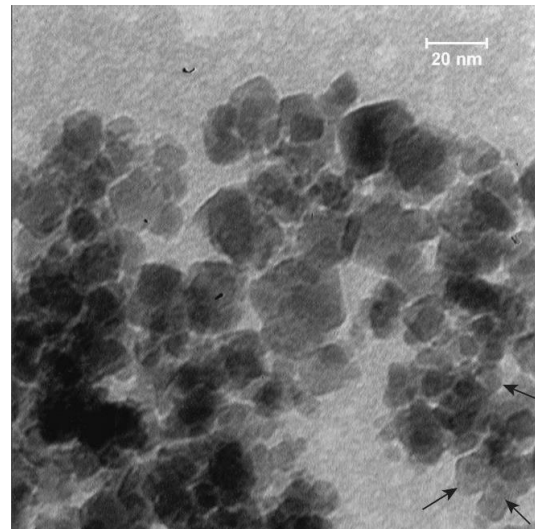


Fig 4. TEM image of dextran@AUR-coated MNPs; the core-shell structure has been shown by arrows

size and high magnetism. Most of the coated nanoparticles had a diameter in the range of 11-16 nm with a mean diameter of 13.643±2.855 nm (Fig. 3c) which is in the typical diameter range for biomedical applications (below 100 nm) [32]. TEM result of dextran@AUR-coated MNPs (Fig. 4) was similar to that of SEM as most of the coated nanoparticles were agglomerated. However, core-shell structure of dextran@AUR-coated MNPs could clearly be seen demonstrating successful coating of Fe₃O₄ nanoparticles.

Dynamic light scattering (DLS) results (Fig. 5a) demonstrated a diameter of 241.4 nm for dextran@AUR-coated MNPs that is substantially different from that of the XRD and SEM results. This is due to adsorption of water molecules on the surface of the coated nanoparticles. Dextran@AUR-coated MNPs had good polydispersity (PDI: 0.188) and a zeta potential of -13.6 mV (Fig. 5b); however, the colloidal ferrofluid was only stable for 10 days at room temperature and small aggregates were seen after this time. The hydrodynamic diameter increased to 291.6 nm (PDI: 0.229) and zeta potential increased to -10.7 mV (Fig. 5c and Fig. 5d), respectively. This can show the occurrence of instability, aggregation and heterogeneity [52]. Low stability of dextran@AUR-coated MNPs may result from two factors, namely the synthesis method and nature of dextran interaction with the surface of MNPs. Although co-precipitation is one of the most efficient ways to synthesize magnetite nanoparticles, it results in the formation of particles

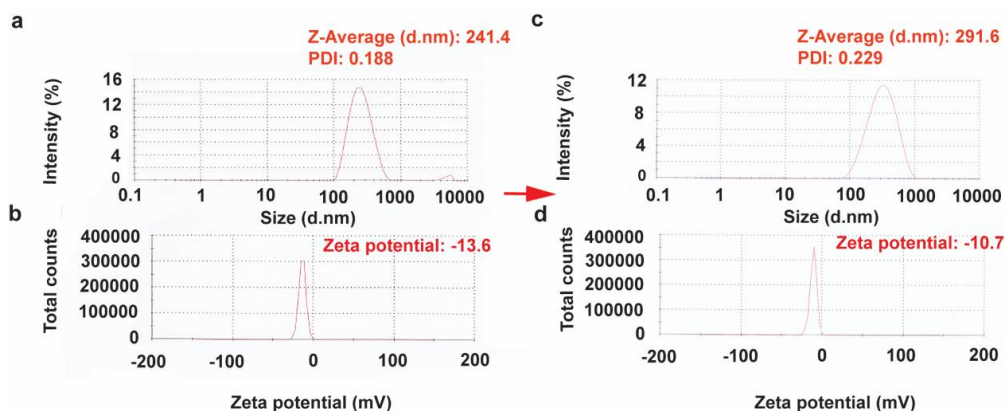


Fig 5. Size distribution by intensity (a) and zeta potential (b) of dextran@AUR-coated MNPs on the first day of synthesis and size distribution by intensity (c) and zeta potential of dextran@AUR-coated MNPs (d) 10 days after synthesis

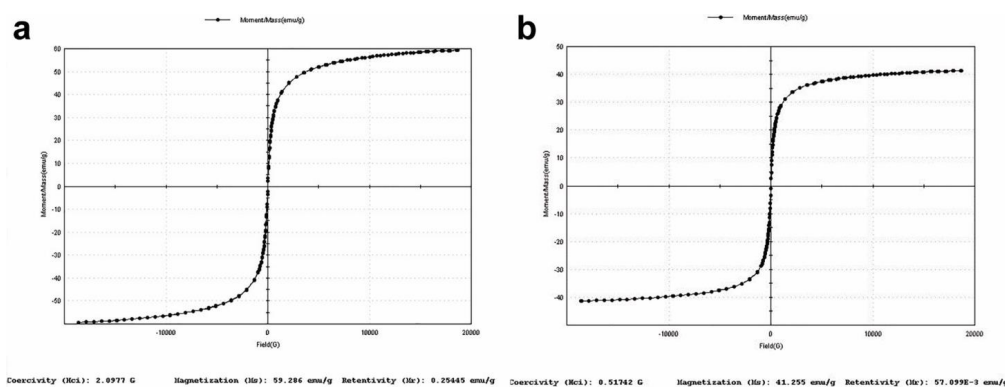


Fig 6. Hysteresis loops for Fe_3O_4 MNPs (a) and dextran@AUR-coated MNPs (b)

with high saturation magnetization (M_s) values which makes their coating and dispersion more difficult in comparison to other synthesis methods such as laser pyrolysis. Further, the hydrogen bonds formed between dextran and the surface of MNPs have a reversible nature resulting in instability and aggregation [53]. To solve this, some researchers have cross-linked dextran shell to make dextran-coated MNPs colloid more stable [43].

VSM measurement was used to analyze magnetic properties. Hysteresis loops of Fe_3O_4 MNPs and dextran@AUR-coated MNPs are shown in Fig 6. The M_s for Fe_3O_4 MNPs and dextran@AUR-coated MNPs are 59.286 and 41.255 emu/g, respectively. Remanence (M_r) and coercivity (H_c) are negligible for uncoated and coated nanoparticles (Table 1), suggesting the superparamagnetic properties of both samples.

The presence of dextran and AUR on the surface of coated nanoparticles has led to a lower

M_s of dextran@AUR-coated MNPs than that of the Fe_3O_4 MNPs [54].

Encapsulation efficiency, drug loading and release test

The encapsulation efficiency and drug loading were calculated according to the standard curve of AUR obtained by UV-Vis spectroscopy and determined to be 10.56% and 6.765%, respectively. It is necessary to mention that low encapsulation and drug loading of AUR is due to the hydrophobic nature of this compound and not instability of

Table 1. Magnetic parameters for Fe_3O_4 MNPs and dextran@AUR-coated MNPs

	M_s (emu/g)	M_r (emu/g)	H_c (G)
Fe_3O_4 MNPs	59.286	0.25445	2.0977
dextran@AUR-coated MNPs	41.255	0.0571	0.51742

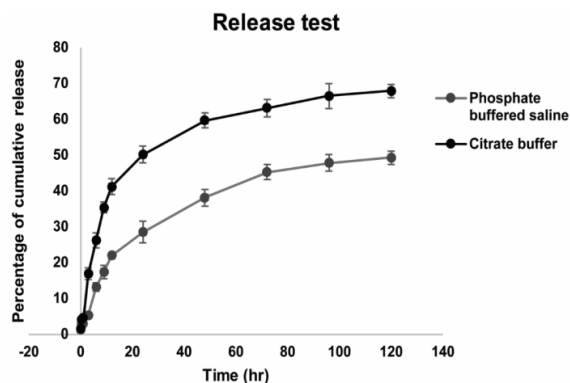


Fig 7. Drug release profile of AUR from dextran@AUR-coated MNPs in PBS (pH= 7.4) and citrate buffer (pH= 5.5)

nanoparticles. The surface of Fe_3O_4 nanoparticles is highly hydrophobic, however, when MNPs are dispersed in aqueous solutions they obtain several OH groups on their surface [55]. Also, dextran is extremely hydrophilic. These hydrophilicities can significantly reduce the effective interactions between the hydrophobic AUR and nanoparticles leading to a low encapsulation efficiency and drug loading. The drug release profile from dextran@AUR-coated MNPs was studied for 120 hours in both physiologic (PBS) and acidic pH (citrate buffer). The percentage of cumulative release (Table S1) was calculated according to the standard curves of AUR obtained by spectrofluorimetry in both PBS and citrate buffer. In PBS buffer, $49.25 \pm 1.84\%$ of the total coated AUR was released after 5 days, however, this percentage was $67.94 \pm 1.85\%$ in citrate buffer (Fig 7). The free drug dissolved immediately after 30 min (Fig. S1), so it is not a suitable anti-cancer drug candidate to be used alone. Dextran@AUR-coated MNPs indicated 28% and 50% of AUR release in pH= 7.4 and 5.5, respectively in 24 hr demonstrating that coated MNPs are not prone to immediate drug release into the plasma.

To compare the release profile of AUR in physiologic and acidic pH, drug release model was fit to Baker-Lonsdale kinetic model. In this model, the best result is achieved when correlation coefficient is close to one. Our results showed that r^2 for pH= 7.4 was 0.97 and for pH= 5.5 was 0.91. The slopes of these models were 0.0015 ± 0.0014 for pH= 7.4 and 0.011 ± 0.0053 for pH= 5.5. Also, the intercepts were 0.00048 ± 0.0003 for pH= 7.4 and 0.001 ± 0.0001 for pH= 5.5. It can be concluded that the release rate of AUR in acidic pH is significantly different from physiologic pH [56].

MDT was equal to 5188 for pH= 7.4 and 7740 for pH= 5.5 indicating a remarkable difference in AUR release kinetics between physiologic and acidic media. Larger AUR release in acidic environment can be advantageous for treating tumor regions.

In vitro cytotoxicity evaluation

AlamarBlue assay was performed to determine the cytotoxicity of different samples and the resulting data were analyzed by GraphPad Prism 5 software. Different groups were compared relative to negative control and significant differences were demonstrated as $*P < 0.05$, $**P < 0.01$, and $***P < 0.001$.

One-way ANOVA analysis results showed that the cytotoxicity of AUR and dextran@ Fe_3O_4 MNPs for PC3, DU145 and LNCaP cell lines was very low at the tested concentrations. Interestingly, dextran@AUR-coated MNPs were significantly cytotoxic for PC3 and LNCaP cells at 5 and 10 $\mu\text{g}/\text{mL}$ and for DU145 at 1, 5 and 10 $\mu\text{g}/\text{mL}$ of final AUR concentration (Fig 8). Dextran@AUR-coated MNPs were more cytotoxic for LNCaP cells (IC_{50} value of 5.737 $\mu\text{g}/\text{mL}$) in comparison to PC3 and DU145 cell lines ($\text{IC}_{50} > 10 \mu\text{g}/\text{mL}$). Two-way ANOVA analysis results showed a remarkable difference in the cytotoxicity of dextran@AUR-coated MNPs in comparison to dextran@ Fe_3O_4 MNPs and AUR (Table S2). This result can represent that the combination of AUR and nanoparticles is responsible for the significant cytotoxic effect of dextran@AUR-coated MNPs to prostate cancer cells. The probable mechanism for enhanced efficacy and cytotoxicity of AUR may be improved penetration of this compound into the cancer cells, not the cytotoxicity of Fe_3O_4 nanoparticles, since effective cellular uptake of MNPs into the target cells has been shown before [57]. Previous studies have demonstrated an increased cytotoxicity of natural compounds to cancer cells when coated on the surface of Fe_3O_4 MNPs. For example, coating the surface of Fe_3O_4 MNPs with umbeliprenin could increase the cytotoxicity of this compound on human fibrosarcoma cell line [58]. Kumar et al. have conjugated quercetin to dextran-coated Fe_3O_4 MNPs for chemotherapy applications. Their results indicated an improved cytotoxicity of conjugated quercetin for MCF-7 cells in comparison to quercetin alone [49]. The cytotoxicity of galbanic acid to prostate cancer cells [59], curcumin to breast cancer cells [60], quercetin to A549 cells [61], and eugenol to

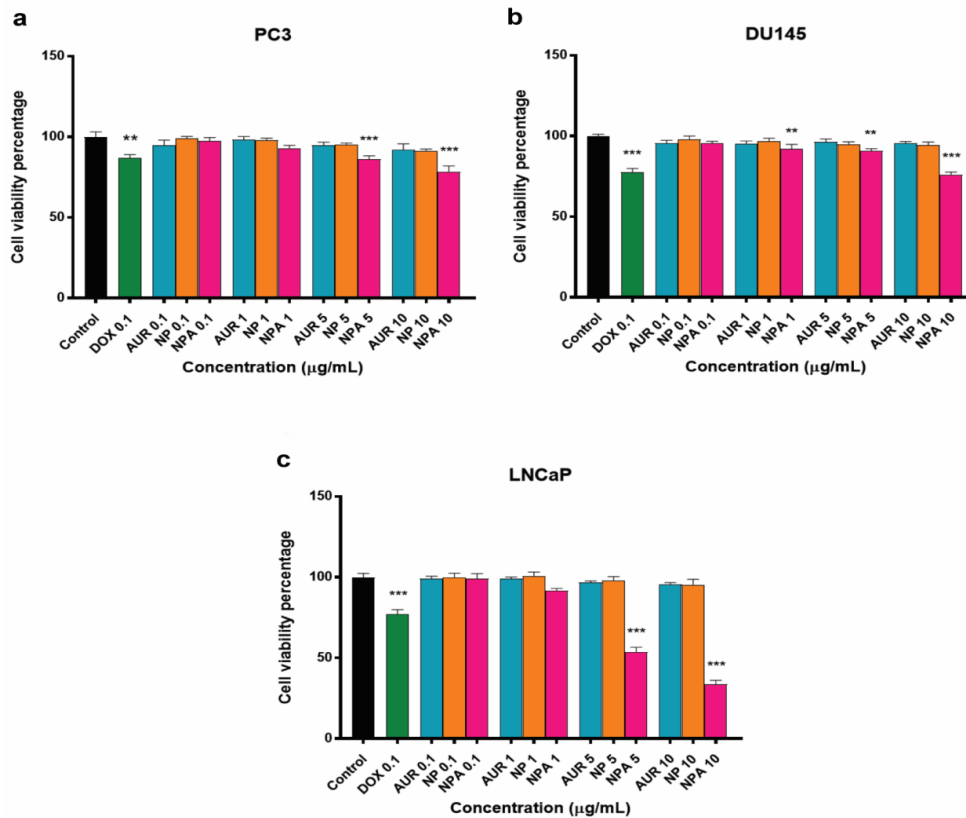


Fig 8. Cytotoxicity of auraptene (AUR), dextran@Fe₃O₄ MNPs (NP) and dextran@AUR-coated MNPs (NPA) on PC3 (a), DU145 (b) and LNCaP (c) cell lines. Untreated cells serve as negative control and doxorubicine (DOX)-treated cells as positive control. Values are mean±SD. Significance of difference is demonstrated as **P*< 0.05, ***P*< 0.01, and ****P*< 0.001 as compared

human glioblastoma astrocytoma [62], has been improved remarkably when coated on the surface of Fe₃O₄ MNPs.

CONCLUSION

In this study, AUR-coated Fe₃O₄ MNPs were synthesized and their cytotoxicity was assessed on PC3, DU145 and LNCaP prostate cancer cells using AlamarBlue test. The nanoparticles had good crystalline structure, relatively spherical shape and superparamagnetic properties and could control AUR release effectively. The cytotoxicity of AUR and dextran@Fe₃O₄ MNPs for prostate cancer cells was very low at the tested concentrations. In contrast, dextran@AUR-coated MNPs could significantly inhibit the proliferation of these cells. We suggest that the enhanced cytotoxicity of AUR-coated MNPs may result from an increased penetration of AUR into the cancer cells. Enhancing the cytotoxic effect of natural compounds with the aid of MNPs can open new horizons in the medicinal applications of nanoparticles. Utilizing

Fe₃O₄ MNPs as drug carriers for anti-cancer natural products can improve the efficacy of these compounds and reduce their side effects. The cytotoxic mechanisms of AUR-coated MNPs and their *in vivo* therapeutic effects are subjects of future work.

ACKNOWLEDGEMENTS

This work was supported by Mashhad University of Medical Sciences Research Council, Mashhad, Iran (grant no. 950959).

CONFLICT OF INTEREST

The authors declare that they have no conflict of interest.

REFERENCES

1. Siegel RL, Miller KD, Jemal A. Cancer Statistics, 2017. *CA Cancer J Clin.* 2017; 67(1): 7-30.
2. Xu J, Zheng SL, Komiya A, Mychaleckyj JC, Isaacs SD, Hu JJ, et al. Germline mutations and sequence variants of the macrophage scavenger receptor 1 gene are associated with prostate cancer risk. *Nat Genet.* 2002; 32(2): 321-325.

3. Nelson WG, De Marzo AM, Isaacs WB. Prostate cancer. *N Engl J Med*. 2003; 349(4): 366-381.
4. Lee JC, Shin EA, Kim B, Kim BI, Chitsazian-Yazdi M, Iranshahi M, et al. Auraptene induces apoptosis via myeloid cell leukemia 1-mediated activation of caspases in PC3 and DU145 prostate cancer cells. *Phytother Res*. 2017; 31(6): 891-898.
5. Soltani F, Mosaffa F, Iranshahi M, Karimi G, Malekaneh M, Haghghi F, et al. Auraptene from *Ferula szowitsiana* protects human peripheral lymphocytes against oxidative stress. *Phytother Res*. 2010; 24(1): 85-89.
6. Kuroyanagi K, Kang MS, Goto T, Hirai S, Ohyama K, Kusudo T, et al. *Citrus auraptene* acts as an agonist for PPARs and enhances adiponectin production and MCP-1 reduction in 3T3-L1 adipocytes. *Biochem Biophys Res Commun*. 2008; 366(1): 219-225.
7. Genovese S, Ashida H, Yamashita Y, Nakgano T, Ikeda M, Daishi S, et al. The interaction of auraptene and other oxyprenylated phenylpropanoids with glucose transporter type 4. *Phytomedicine*. 2017; 32: 74-79.
8. Nishimoto S, Muranaka A, Nishi K, Kadota A, Sugahara T. Immunomodulatory effects of *Citrus* fruit auraptene *in vitro* and *in vivo*. *J Funct Foods*. 2012; 4(4): 883-890.
9. Askari VR, Baradaran Rahimi V, Rezaee SA, Boskabady MH. Auraptene regulates Th1/Th2/TReg balances, NF-kappaB nuclear localization and nitric oxide production in normal and Th2 provoked situations in human isolated lymphocytes. *Phytomedicine*. 2018; 43: 1-10.
10. Fiorito S, Epifano F, Preziuso F, Cacciatore I, di Stefano A, Taddeo VA, et al. Natural oxyprenylated coumarins are modulators of melanogenesis. *Eur J Med Chem*. 2018; 152: 274-282.
11. Niu X, Huang Z, Zhang L, Ren X, Wang J. Auraptene has the inhibitory property on murine T lymphocyte activation. *Eur J Pharmacol*. 2015; 750: 8-13.
12. Okuyama S, Minami S, Shimada N, Makihata N, Nakajima M, Furukawa Y. Anti-inflammatory and neuroprotective effects of auraptene, a *Citrus* coumarin, following cerebral global ischemia in mice. *Eur J Pharmacol*. 2013; 699: 118-123.
13. Ghanbarabadi M, Iranshahi M, Amoueian S, Mehri S, Motamedshariaty VS, Mohajeri SA. Neuroprotective and memory enhancing effects of auraptene in a rat model of vascular dementia: Experimental study and histopathological evaluation. *Neurosci Lett*. 2016; 623: 13-21.
14. Nakajima M, Shimizu R, Furuta K, Sugino M, Watanabe T, Aoki R, et al. Auraptene induces oligodendrocyte lineage precursor cells in a cuprizone-induced animal model of demyelination. *Brain Res*. 2016; 1639: 28-37.
15. Kawabata K, Murakami A, Ohigashi H. *Citrus auraptene* targets translation of MMP-7 (matrilysin) via ERK1/2-dependent and mTOR-independent mechanism. *FEBS Lett*. 2006; 580(22): 5288-5294.
16. Krishnan P, Yan KJ, Windler D, Tubbs J, Grand R, Li BD, et al. *Citrus auraptene* suppresses cyclin D1 and significantly delays N-methyl nitrosourea induced mammary carcinogenesis in female Sprague-Dawley rats. *BMC Cancer*. 2009; 9: 259.
17. Krishnan P, Kleiner-Hancock H. Effects of auraptene on IGF-1 stimulated cell cycle progression in the human breast cancer cell line, MCF-7. *Int J Breast Cancer*. 2012; 2012: 502092.
18. Tang M, Ogawa K, Asamoto M, Hokaiwado N, Seeni A, Suzuki S, et al. Protective effects of *Citrus nobilitein* and auraptene in transgenic rats developing adenocarcinoma of the prostate (TRAP) and human prostate carcinoma cells. *Cancer Sci*. 2007; 98(4): 471-477.
19. Chenthamara D, Subramaniam S, Ramakrishnan SG, Krishnaswamy S, Essa MM, Lin FH, et al. Therapeutic efficacy of nanoparticles and routes of administration. *Biomater Res*. 2019; 23(1): 20.20. Patra JK, Das G, Fraceto LF, Campos EVR, Rodriguez-Torres MDP, Acosta-Torres LS, et al. Nano based drug delivery systems: Recent developments and future prospects. *J Nanobiotechnol*. 2018; 16: 71.
21. He X, Hwang HM. Nanotechnology in food science: Functionality, applicability, and safety assessment. *J Food Drug Anal*. 2016; 24: 671-681.
22. Jeevanandam J, Barhoum A, Chan YS, Dufresne A, Danquah MK. Review on nanoparticles and nanostructured materials: History, sources, toxicity and regulations. *Beilstein J Nanotechnol*. 2018; 9: 1050-1074.
23. Rao PV, Nallappan D, Madhavi K, Rahman S, Jun Wei L, Gan SH. Phytochemicals and biogenic metallic nanoparticles as anticancer agents. *Oxid Med Cell Longev*. 2016; 2016: 3685671.
24. Hernández-Hernández AA, Aguirre-Álvarez G, Cariño-Cortés R, Mendoza-Huizar LH, Jiménez-Alvarado R. Iron oxide nanoparticles: Synthesis, functionalization, and applications in diagnosis and treatment of cancer. *Chem Pap*. 2020; 74: 3809-3824.
25. Wu W, Wu Z, Yu T, Jiang C, Kim WS. Recent progress on magnetic iron oxide nanoparticles: Synthesis, surface functional strategies and biomedical applications. *Sci Technol Adv Mater*. 2015; 16: 023501.
26. Vangijzegem T, Stanicki D, Boutry S, Paternoster Q, Vander Elst L, Muller RN, et al. VSION as high field MRI T1 contrast agent: Evidence of their potential as positive contrast agent for magnetic resonance angiography. *Nanotechnology*. 2018; 29: 265103.
27. Pham HN, Pham THG, Nguyen DT, Phan QT, Le TTH, Ha PT, et al. Magnetic inductive heating of organs of mouse models treated by copolymer coated Fe3O4 nanoparticles. *Adv Nat Sci Nanosci Nanotechnol*. 2017; 8: 025013.
28. Gupta AK, Gupta M. Synthesis and surface engineering of iron oxide nanoparticles for biomedical applications. *Biomaterials*. 2005; 26: 3995-4021.
29. Vangijzegem T, Stanicki D, Laurent S. Magnetic iron oxide nanoparticles for drug delivery: Applications and characteristics. *Expert Opin Drug Deliv*. 2019; 16: 69-78.
30. Parveen S, Misra R, Sahoo SK. Nanoparticles: A boon to drug delivery, therapeutics, diagnostics and imaging. *Nanomedicine*. 2012; 8: 147-166.
31. Teja AS, Koh PY. Synthesis, properties, and applications of magnetic iron oxide nanoparticles. *Prog Cryst Growth Charact Mater*. 2009; 55: 22-45.
32. Laurent S, Forge D, Port M, Roch A, Robic C, Vander Elst L, et al. Magnetic iron oxide nanoparticles: Synthesis, stabilization, vectorization, physicochemical characterizations, and biological applications. *Chem Rev*. 2008; 108: 2064-2110.
33. Ali A, Zafar H, Zia M, Ul Haq I, Phull AR, Ali JS, et al. Synthesis, characterization, applications, and challenges of iron oxide nanoparticles. *Nanotechnol Sci Appl*. 2016; 9: 49-67.

34. Zamani H, Rastegari B, Varamini M. Antioxidant and anti-cancer activity of *Dunaliella salina* extract and oral drug delivery potential via nano-based formulations of gum Arabic coated magnetite nanoparticles. *J Drug Deliv Sci Technol.* 2019; 54: 101278.
35. Soshnikova YM, Roman SG, Chebotareva NA, Baum OI, Obrezkova MV, Gillis RB, et al. Starch-modified magnetite nanoparticles for impregnation into cartilage. *J Nanopart Res.* 2013; 15: 2092.
36. Nadeem M, Ahmad M, Akhtar MS, Shaari A, Riaz S, Naseem S, et al. Magnetic properties of polyvinyl alcohol and doxorubicine loaded iron oxide nanoparticles for anticancer drug delivery applications. *PloS One.* 2016; 11(6): e0158084.
37. Viali WR, da Silva Nunes E, dos Santos CC, da Silva SW, Aragón FH, Coaquira JAH, et al. PEGylation of SPIONs by polycondensation reactions: A new strategy to improve colloidal stability in biological media. *J Nanopart Res.* 2013; 15: 1824.
38. Tai MF, Lai CW, Abdul Hamid SB. Facile synthesis polyethylene glycol coated magnetite nanoparticles for high colloidal stability. *J Nanomater.* 2016; 2016: 8612505.
39. Zeinali S, Nasirimoghaddam S, Sabbaghi S. Investigation of the synthesis of chitosan coated iron oxide nanoparticles under different experimental conditions. *Int J Nanosci Nanotechnol.* 2016; 12(3): 183-190.
40. Unsoy G, Yalcin S, Khodadust R, Gunduz G, Gunduz U. Synthesis optimization and characterization of chitosan-coated iron oxide nanoparticles produced for biomedical applications. *J Nanopart Res.* 2012; 14: 964.
41. Shagholani H, Ghoreishi SM. Investigation of tannic acid cross-linked onto magnetite nanoparticles for applying in drug delivery systems. *J Drug Deliv Sci Technol.* 2017; 39: 88-94.
42. Regmi R, Gumber V, Subba Rao V, Kohli I, Black C, Sudakar C, et al. Discrepancy between different estimates of the hydrodynamic diameter of polymer-coated iron oxide nanoparticles in solution. *J Nanopart Res.* 2011; 13: 6869-6875.
43. Unterweger H, Dézsi L, Matuszak J, Janko C, Poettler M, Jordan J, et al. Dextran-coated superparamagnetic iron oxide nanoparticles for magnetic resonance imaging: Evaluation of size-dependent imaging properties, storage stability and safety. *Int J Nanomedicine.* 2018; 13: 1899-1915.
44. Liu G, Hong RY, Guo L, Liu GH, Feng B, Li YG. Exothermic effect of dextran-coated Fe₃O₄ magnetic fluid and its compatibility with blood. *Colloid Surf A Physicochem Eng Asp.* 2011; 380: 327-333.
45. Tartaj P, Morales MP, Veintemillas-Verdaguer S, Gonzalez-Carreno T, Serna CJ. Synthesis, properties and biomedical applications of magnetic nanoparticles. In: Buschow KHJ, editor. *Handbook of Magnetic Materials.* Amsterdam, Netherlands: Elsevier; 2006. p. 403.
46. U.S. Department of Health and Human Services, Food and Drug Administration, Center for Drug Evaluation and Research. Extended release oral dosage forms: Development, evaluation, and application of in vitro/in vivo correlations. *FDA Maryland* 1997; pp. 1-27.
47. Lakay E. Superparamagnetic iron oxide based nanoparticles for the separation and recovery of precious metals from solution [dissertation]. Stellenbosch, University of Stellenbosch. 2009.
48. Haw CY, Chia CH, Zakaria S, Mohamed F, Radiman S, Teh CH, et al. Morphological studies of randomized dispersion magnetite nanoclusters coated with silica. *Ceram Int.* 2011; 37(2): 451-64.
49. Rajesh Kumar S, Priyatharshni S, Babu VN, Mangalaraj D, Viswanathan C, Kannan S, et al. Quercetin conjugated superparamagnetic magnetite nanoparticles for *in-vitro* analysis of breast cancer cell lines for chemotherapy applications. *J Colloid Interface Sci.* 2014; 436: 234-242.
50. Daneshmand S, Jaafari MR, Movaffagh J, Malaek-Nikouei B, Iranshahi M, Seyedian Moghaddam A, et al. Preparation, characterization, and optimization of auraptene-loaded solid lipid nanoparticles as a natural anti-inflammatory agent: *In vivo* and *in vitro* evaluations. *Colloids Surf B Biointerfaces.* 2018; 164: 332-339.
51. Almahy HA, Alagimi AA. Coumarins from the roots of *Cleome Viscosa* (L.) antimicrobial and cytotoxic studies. *Arab J Chem.* 2012; 5: 241-244. doi: 10.1016/j.arabjc.2011.03.019
52. Riddick TM. *Control of colloid stability through zeta potential.* Wynnewood, USA: Livingston Publishing Co.; 1968.
53. Carmen Bautista M, Bomati-Miguel O, del Puerto Morales M, Serna CJ, Veintemillas-Verdaguer S. Surface characterisation of dextran-coated iron oxide nanoparticles prepared by laser pyrolysis and coprecipitation. *J Magn Magn Mater.* 2005; 293: 20-27.
54. Fu W, Yang H, Hari B, Liu S, Li M, Zou G. Preparation and characteristics of core-shell structure cobalt/silica nanoparticles. *Mater Chem Phys.* 2006; 100: 246-250.
55. Woo K, Hong J. Surface modification of hydrophobic iron oxide nanoparticles for clinical applications. *IEEE Trans Magn.* 2005; 41: 4137-4139.
56. Costa P, Sousa Lobo JM. Modeling and comparison of dissolution profiles. *Eur J Pharm Sci.* 2001; 13: 123-133.
57. Sato A, Itcho N, Ishiguro H, Okamoto D, Kobayashi N, Kawai K, et al. Magnetic nanoparticles of Fe₃O₄ enhance docetaxel-induced prostate cancer cell death. *Int J Nanomedicine.* 2013; 8: 3151-3160.
58. Khorramizadeh MR, Esmail-Nazari Z, Zarei-Ghaane Z, Shakibaie M, Mollazadeh-Moghaddam K, Iranshahi M, et al. Umbelliprenin-coated Fe₃O₄ magnetite nanoparticles: Antiproliferation evaluation on human fibrosarcoma cell line (HT-1080). *Mater Sci Eng C.* 2010; 30: 1038-1042.
59. Mohtashami L, Ghows N, Tayarani-Najaran Z, Iranshahi M. Galbanic acid-coated Fe₃O₄ magnetic nanoparticles with enhanced cytotoxicity to prostate cancer cells. *Planta Med.* 2019; 85: 169-178.
60. Yallapu MM, Othman SF, Curtis ET, Bauer NA, Chauhan N, Kumar D, et al. Curcumin-loaded magnetic nanoparticles for breast cancer therapeutics and imaging applications. *Int J Nanomedicine.* 2012; 7: 1761-1779.
61. Verma NK, Crosbie-Staunton K, Satti A, Gallagher S, Ryan KB, Doody T, et al. Magnetic core-shell nanoparticles for drug delivery by nebulization. *J Nanobiotechnol.* 2013; 11: 1.
62. Shahabadi N, Akbari A, Karampour F, Falsafi M. Cytotoxicity and antibacterial activities of new chemically synthesized magnetic nanoparticles containing eugenol. *J Drug Deliv Sci Technol.* 2019; 49: 113-122.